Toughening of epoxies by covalently anchoring triazole-functionalized stacked-cup carbon nanofibers

Wanshuang Liu, Junhua Kong, Weilong Eric Toh, Rui Zhou, Guoqiang Ding, Shu Huang, Yuliang Dong, Xuehong Lu*

School of Materials Science and Engineering, Nanyang Technological University, 50 Nanyang Avenue, Singapore 639798, Singapore

*Corresponding author: Tel: +65 9847 6690
E-mail address: asxhlu@ntu.edu.sg (X. Lu)

Abstract: Novel triazole-functionalized carbon nanofibers (m-CNFs) were prepared by one-step arylation with diazonium salts generated in situ. Microscopic observations indicate that m-CNFs exhibit significantly improved dispersibility in a high-performance epoxy resin compared with pristine CNFs (p-CNFs). The results of DSC and SEM show evidence of interfacial reaction and a more robust interface between m-CNFs and the epoxy matrix. Thermal and mechanical properties of two CNF/epoxy composites were systematically studied at different filler loadings. The results show that both CNF fillers could reinforce the epoxy matrix without sacrificing their thermal properties. Benefiting from the improved dispersibility and interfacial interaction, the ability of m-CNFs in toughening the epoxy resin is clearly superior to p-CNFs. The addition of only 0.4 wt% m-CNFs gives 41 and 80% enhancement in critical stress intensity factor (K_{IC}) and the critical strain energy release rate (G_{IC}), respectively.

Keywords: Carbon nanofibers; A. Polymer-matrix composites (PMCs); B. Fracture toughness; B. Interface; B. Thermomechanical properties

1. Introduction

Toughening of brittle epoxy thermosets has long been a subject of intense research since the inherent brittleness and poor resistance to crack propagation of epoxy resins greatly restrict their widespread applications in industries. The incorporation of a second phase, either rigid or soft, into epoxy matrices is presently a well-established strategy for improving the fracture toughness of epoxies. In these systems, phase-separated morphology can initiate various toughening mechanisms to dissipate a portion of energy available for crack propagation [1,2]. To date, the use of numerous micro-sized and nano-sized second phases such as rubber [3], thermoplastics [4], ceramic particles [5], carbon-based nanomaterials [6-8] and their combinations [9-12] in toughening epoxy thermosets has been demonstrated.

Recently, the potential applications of stacked-cup carbon nanofibers (CNFs) as reinforcing fillers for polymer-based composites have attracted considerable attention due to its nanoscale diameter, high aspect ratio, and excellent instinct mechanical, thermal and electrical properties. Although the overall properties of the CNFs are slightly inferior to those of carbon nanotubes (CNTs), the manufacturing cost of CNFs are much lower (about 3-500 times lower than that of CNTs) [13,14]. More importantly, Brinson et al. recently demonstrated that the unique stacked-cup structure of CNFs can bring out sacrificial bonding behaviors, which are not found in the systems with CNTs or graphene [15]. Their mechanical testing results revealed that the addition of only 0.68 wt % stacked-cup CNFs would increase the critical strain energy release rate (G_{IC}) by approximately 43-112% in reinforcing epoxy resins with various blend.

There is, however, still a strong need to further enhance the toughening efficiency of CNFs. The challenges of achieving optimum properties of epoxy/CNF composites at even lower CNF loadings lie primarily in two areas. One is that CNFs tend to agglomerate in epoxy matrices due

to their high aspect ratio and surface energy, leading to inhomogeneous dispersion. The other is the lack of interfacial forces between CNFs and epoxy matrices so that the CNFs can be easily pulled out, lowering the efficiency of load transfer from the matrices to the reinforcement [16-18]. In general, covalent incorporation of CNFs into epoxies through chemical modification and functionalization of CNFs is considered to be a feasible method for solving the above issues as it can both provide chemical affinity for efficient dispersion and improve interfacial interactions through chemical bonding. Several functionalization methods for CNFs have already been reported, such as carbonylation by Friedel–Crafts (F–C) reaction [13,19], carboxylation by strong acid (HNO_3 or/and H_2SO_4) as well as subsequent functionalization [20-22]. Although all these functionalized CNFs show improved dispersibility and interfacial interactions in epoxy matrices and thus give rise to significantly enhanced stiffness, their toughening effects have not yet been reported in literature to the best of our knowledge. Therefore, there remains a need to clarify whether the interfacial chemical bonds would really have significant influence on fracture toughness of the CNF-reinforced epoxy composites.

Motivated by the aforementioned issues, we prepared novel triazole-functionalized CNFs (m-CNFs) by one-step arylation with diazonium salts generated in situ. Unlike the modification using strong acid, this method is milder and less destructive to the CNF structure, allowing the CNFs to maintain their good intrinsic properties. The m-CNFs were subsequently introduced into an aerospace-grade anhydride-cured epoxy resin. The grafted triazole groups could initiate localized curing reaction directly from the surfaces of m-CNFs and thus the modified CNFs could be covalently anchored onto the epoxy network during the cure process [23]. Thermal and mechanical properties of the CNF/epoxy composites were systematically investigated. Pristine CNF (p-CNF)/epoxy composites and neat epoxy samples were also prepared as reference

materials in order to study the influences of functionalization on the dispersion state of CNFs and interfacial interaction between CNFs and epoxy matrix, which are closely related to the stiffening and toughening efficiencies of CNFs.

2. Experimental

2.1. Materials

Pyrograf-III CNFs (PR-24-XT-LHT) with diameter of 70–200 nm and length of 50-200 μm were obtained from Applied Science Inc. (USA). All solvents and reagents were purchased from Sigma-Aldrich Chemicals Inc. (USA) and used as received, unless otherwise specified. 1-(4-Aminobenzyl)-1,2,4-triazole was purchased from Combi-Blocks Inc (USA). Tetra-functional epoxy (Resin XB 9721) and anhydride hardener (Aradur® 917) were supplied by Huntsman Advanced Materials (USA). Zinc acetylacetonate was used as catalyst (or so-called accelerator) and supplied by Sigma-Aldrich Chemicals Inc. (USA). The chemical structures of Resin XB 9721 and Aradur® 917 are given in Fig. 1.

2.2. Synthesis of m-CNFs

In a typical experiment, 0.5 g of p-CNFs were dipped into 150 ml of DMF, and sonicated in an ultrasonic bath for 2 h. Separately, 1-(4-aminobenzyl)-1,2,4-triazole (9.1 g, ≈4 equiv/mol of carbon) was dissolved in 150 ml acetonitrile, and then this arylamine solution was added in the CNF suspension. After degassing with argon for 30 min, isoamyl nitrite (10.7 ml) was quickly added by a syringe and the suspension was stirred at 60 °C for about 15 h in an argon atmosphere. After cooling to room temperature, the suspension was filtered using a PTFE (0.45 μm) membrane and washed extensively with DMF. The functionalized CNFs were further purified by repeated sonication and washing with DMF, and then acetone. Finally, the obtained m-CNFs were dried in a vacuum oven at 60 °C for 48 h.

2.3. Preparation of CNF/Epoxy composites

A desired amount of p-CNFs or m-CNFs were first dispersed in low viscosity anhydride hardener, and the mixture was sonicated using a Sonic & Materials model VCX-750 (1 cm^2 Ti horn at 20 kHz, 750 Watts) at 50% amplitude for 30 min (pulse: 2s on and 2s off) in an ice bath. Then, the mixture was subjected to a bath sonication for another 4 h. Separately, epoxy monomer and catalyst (1 wt% of the total weight) were mixed homogeneously with rotary evaporator at 80 °C for half an hour. Then, all the components were uniformly mixed together and the weight ratio of epoxy/hardener was 100/141 as recommended by the supplier. Finally, the mixture was poured into a self-made silicone mold and degassed for 1 h at a vacuum approaching about 0.1 mbar. All samples were cured using the following profile: 120 °C for 2 h, 160 °C for 2 h and 200 °C for 2 h. Samples for mechanical testing were obtained by curing in the silicone mold with specific dimensions.

2.4. Characterization

Fourier transform infrared (FTIR) spectra were obtained using a Perkin Elmer Instruments Spectrum GX FTIR spectrometer at room temperature in a wave-number range from 600 to 4000 cm^{-1}. All of the samples were prepared as pellets using spectroscopic grade KBr. X-ray photoelectron spectroscopy (XPS) measurements were performed on a Kratos Analytical AXIS His spectrometer with a monochromatized Al Ka X-ray source (1486.6 eV photons) and Shirley functions were used to correct the baseline. Elemental analysis was performed using a Perkin Elmer Instruments CHNS-O Analyzer. The weight percentage (%) composition of Carbon, Hydrogen and Nitrogen were measured. Differential scanning calorimetry (DSC) was recorded on a TA Instruments DSC Q10 using N_2 as purge gas at a heating rate 3 °C/min. Thermal gravimetric analysis (TGA) were performed on a TA Instruments TGA Q 500 under a nitrogen

or air atmosphere over a temperature range of 25 - 800 °C at a heating rate of 10 °C/min. Dynamic mechanical analysis (DMA) was conducted on a TA Instruments DMA Q800 at a heating rate of 3 °C/min and frequency of 1 Hz under an air atmosphere. The tests were carried out using the single cantilever mode on the specimens with dimension of 40 × 13.0 × 2.0 mm^3. Tensile tests were performed using an ITW Instron Tester 5567 with a 3 kN load cell at a crosshead speed of 1 mm/min. The dog-bone shaped tensile samples were prepared according to the ASTM D638 standard. Each reported value was the average of at least six specimens. Fracture toughness of the composites was measured according to ASTM D5045 standard using a three-point-bend (SEN-3PB) single edge-notch specimen with geometry of 53×12×6 mm^3. A sharpened notch was machined at the midpoint of each specimen by a fine band saw. A pre-crack was then initiated by tapping a fresh razor blade in the notch. Specimens were loaded to failure at a crosshead speed of 1 mm/min using an Instron Micro Tester 5848 equipped with a 2 kN load cell. K_{IC} (critical stress intensity factor) and G_{IC} (critical strain energy release rate) were calculated in accordance to ASTM D 5045 standard. Each reported value was the average of at least six specimens. The fracture surface morphologies of the tensile bars were investigated by a JEOL FESEM 7600F field emission scanning electron microscope (FESEM). The samples were coated with gold for 100 sec. Transmission electron microscopy (TEM) was performed on a JEOL-2010 with accelerating voltage of 200 kV. For CNF/epoxy composites, the samples were prepared by ultramicrotome with a thickness of 50-70 nm at room temperature in water.

3. Results and discussion

3.1. Synthesis and characterization of m-CNFs

Arylation with diazonium salts generated in situ, which was originally developed by Tour's group [24], has been found to be an efficient and mild method for the functionalization of nano-

carbon materials like CNTs or graphene [10,25]. The CNFs (PR-24-XT-LHT) used in this study has a morphology termed stacked cup or cone helix with sloping parallel edge planes piling along the fiber axis, and a minimal and ordered chemically vapor deposited layer of carbon on the surface. These exposed graphene edge planes are rather reactive and can be readily modified through chemical functionalization [26], which makes it feasible to functionalize CNFs through the above-mentioned arylation approach. Fig. 1 illustrates the synthesis route of m-CNFs used in this study.

The structure of m-CNFs was characterized by various analytical methods. Figs. 2a-c shows the XPS spectra of p-CNFs and m-CNFs. The high-resolution C1s XPS spectra reveals that p-CNFs primarily consist of one type of carbon (C=C) at 285.0 ev (Fig. 2a). The very faint bands between 286.0 and 288.0 ev can be attributed to a small amount of C-O formed by the oxidation of p-CNF surface in ambient environment. After arylation, new C 1s peaks corresponding to C-N and C=N appear at 286.9 and 285.8 ev, respectively (Fig. 2b) [27]. Moreover, nitrogen-related bands at 399.6 and 401.4 ev, arising from C-N and C=N in the triazole ring [28,29], appear in the deconvoluted N1s XPS spectra of m-CNFs (Fig. 2c). The results of FTIR studies (Fig. 2d) further confirm the successful functionalization of the surface of m-CNFs. As expected, there are almost no other specific bands in the FTIR spectrum of p-CNFs, except a band at ca 1580 cm^{-1} corresponding to the graphite structure [21] and a broad band between 1000 and 1300 cm^{-1} ascribed to the weak surface oxidation of p-CNFs. The vibration band at ca 3420 cm^{-1} for both p-CNFs and m-CNFs can be attributed to the absorbed water. By contrast, new bands at 2960 cm^{-1} (symmetric stretching band of C-H), 1515, 1380, and 1265 cm^{-1} (stretching bands of C-N and bending bands of C-H in triazole) [30,31] appear in the FTIR spectrum of m-CNFs.

TGA and elemental analysis were conducted to further estimate the grafting efficiency. Fig. 2e shows the TGA results of p-CNFs and m-CNFs in a nitrogen atmosphere. The weight loss of p-CNFs is less than 1% as it is robust under nitrogen atmosphere, whereas m-CNFs lose *ca* 9% of the total weight at 800 °C. A slight weight loss is detected up to 100 °C, which corresponds to the residual absorbed moisture because of the polarity of triazole group. The weight loss can be mainly attributed to the decomposition of the functional groups attached to the CNF surface. Elemental analysis results (Table S1 in Supplementary materials) show that the nitrogen content in m-CNFs is about 3.0 wt%. As all the nitrogen atoms should come from the triazole compound, the weight percent of the grafted triazole is estimated to be about 11 %, which is close to the result of TGA.

3.2. Effects of functionalization on curing behaviors

Tertiary amines have been widely used as cure catalyst or accelerator for epoxy/anhydride systems. Tertiary amines are generally considered to react with epoxy and anhydride groups, yielding active carboxylate and alkoxide anions that initiate an alternating copolymerization between epoxy and anhydride [32,33]. The influence of the grafted triazole groups on the curing behaviors of the epoxy/anhydride system was investigated by DSC. As shown in Figs. S1a-c in Supplementary materials, the addition of zinc acetylacetonate as catalyst distinctly decreases the exothermal peak temperature and the addition of p-CNFs seems to have minimal effects on the curing reaction. However, the DSC plot of m-CNF/epoxy system with catalyst shows multi-exothermal peak in the temperature range of 120-170 °C (Fig. S1d in Supplementary materials), indicating the combined catalytic effects of zinc acetylacetonate and grafted triazole groups. The exotherms of different epoxy systems (Table S2 in Supplementary materials) provide further evidence of the interfacial reaction between m-CNFs and epoxy matrix. In case of no additional

catalyst, the m-CNF/epoxy system shows an increased exotherm compared with that of neat epoxy system, indicating that the grafted triazole groups on the m-CNF surface participate in the curing reaction through catalyzing. When catalyst is added, the addition of m-CNFs is observed to decrease the curing rate, which may be due to the poor mobility of epoxy segments initiated from the surface of bulk m-CNFs. Finally, after completing the cure profile, the samples were reheated to 280 °C in DSC. The exotherm in Table S3 in Supplementary materials is considered to correspond to the reaction of residual functional groups that didn't react during post curing. Although the addition of m-CNFs has disturbed the curing reaction similar to other researcher's finding in functionalized CNT/epoxy system [34,35], two composites show lower exotherm in reheating than that of neat epoxy, indicating the final cure degree is not decreased by addition of the two types of CNFs. This result is consist with the past report [15] and will be further indirectly verified through DMA later.

3.3. Mechanical properties

Tensile and fracture toughness tests were performed to determine the mechanical properties of neat epoxy resin and the composites in order to evaluate the effectiveness of this functionalization strategy. The tensile properties of neat epoxy resin and two series of composites are summarized in Figs. 3a-b. Compared with neat epoxy resin, the addition of p-CNFs and m-CNFs improves both the tensile strength and Young's modulus of resulting composites as filler loading increases up to 0.4 wt%. The average tensile strength and Young's modulus of neat epoxy resin are 39.0 and 3407 MPa, respectively. The incorporation of 0.4 wt% p-CNFs and m-CNFs gives about 12.0 and 27.7% increase in tensile strength, 7.7 and 8.2% increase in Young's modulus, respectively.

The toughness is an important property for thermosetting polymers, especially for multi-functional epoxy resin with a high crosslinking density. The results of the fracture toughness tests are shown in Figs. 3c-d. Similar to the trend of tensile tests, the fracture toughness of two series of composites increases with the increasing of filler loading up to 0.4 wt%. Compared with the neat epoxy resin, the incorporation of 0.4 wt% p-CNFs and m-CNFs increases the critical stress intensity factor (K_{IC}) by approximately 27 and 41%, the critical strain energy release rate (G_{IC}) by 46 and 80%, respectively. The test data plotted in Fig. 3 are summarized in Table S4 in Supplementary materials. Evidently, the ability of m-CNFs in toughening the epoxy resin is superior to that of p-CNFs. Toughening mechanisms of p-CNFs reinforced epoxy composites have been investigated in detail in a past report [15]. Herein, our emphasis is placed upon the effects of surface functionalization on the state of dispersion and interfacial interaction between CNFs and epoxy matrix, which may be the origin of the differences in toughening efficiency between the two CNF fillers.

There are two key challenges to achieve good dispersion of CNF fillers in an epoxy matrix. One is to disperse bundled CNFs into individual CNF. The other is to maintain the uniform dispersion state during the curing process, because the viscosity of epoxy matrix is significantly reduced with the increase of temperature at the initial stage of curing process, which will facilitate the CNFs to re-agglomerate. A simple test to examine the functionalization effects on the filler/matrix miscibility was conducted by inspection of CNF/epoxy blends using an optical microscope (Nikon Eclipse LV100). Figs. 4a-d display the representative optical micrographs showing the dispersion states of the two types of CNF fillers in the epoxy matrix before and after curing. Before observation, both samples with 0.4 wt% filler loading were sonicated in a bath sonication for 12 h to ensure the adequate dispersion. As can be observed, p-CNFs tend to

agglomeration in the epoxy matrix regardless of whether the system is cured (Figs. 4a and c). By contrast, m-CNFs can be well dispersed in the epoxy/anhydride mixture before curing and form only very small aggregates during the cure process owing to the surface functionalization (Figs. 4b and d).

To further investigate the dispersion state of CNFs in the epoxy matrix, ultrathin sections of the composites with 0.4 wt% filler loading were examined by TEM. Agglomerated bundles of p-CNFs can be observed in the epoxy matrix (Fig. 4e), consistent with the result of optical microscopy. In the case of m-CNFs, the surface functionalization facilitates the dispersion of m-CNFs in the epoxy matrix and most of the m-CNFs observed are well separated with one another (Fig. 4f).

Fig. 5 shows the representative SEM micrographs obtained from fractured surfaces of neat epoxy resin and the composites with 0.4 wt% filler loading. The neat epoxy resin shows smooth and mirror-like fractured surfaces, indicating a brittle failure mode without any ductility (Figs. 5a and b). Figs. 5c and d show the typical fracture surfaces of p-CNF/epoxy composites (cf. Supplementary materials Fig. S2 for more SEM micrographs). Debonded CNFs are clearly discernable on the fractured surfaces, revealing that p-CNFs and the epoxy matrix are not well bonded. In sharp contrast to p-CNFs, most of m-CNFs are observed to be embedded in the epoxy resin and the interfacial boundary becomes indistinct (Fig. 5f and Fig. 6), indicating a robust interfacial interaction between m-CNFs and the epoxy matrix brought about by the chemical bonding.

In order to gain insight into the effects of the interfacial chemical bonds on toughening mechanism, SEM micrographs in Fig. 6 show typical features of the fractured surfaces from m-CNF/epoxy composites. Similar to CNT-reinforced epoxy composites [36-38], evidence of

toughening caused by crack bridging, fiber rupture, pullout and local debonding can be observed (Figs. 6a-c), while different from CNT-reinforced epoxy composites, some broken CNFs with sharp tips can be observed, as shown by arrow in Figure 6d and inset, which are likely to be caused by the unraveling of the graphene layers of the stacked-cup CNFs and related to a sacrificial bonding mechanism [15]. By comparing the morphologies of the fractured surfaces of the m-CNF and p-CNF reinforced composites, it is clear that improved interfacial interaction and dispersibility between m-CNFs and the epoxy matrix contribute to dissipating more energy for crack propagation through the mechanisms mentioned above.

3.4. Thermal and thermo-mechanical properties

The dynamic mechanical properties of neat epoxy resin and composites were investigated by DMA. The storage modulus (*E'*), loss modulus (*E''*) and tan δ versus temperature curves are given in Fig. 7 and the data are summarized in Table 1. Storage modulus reflects the elastic properties or the energy storage in the composites. Both series of composites exhibit increased *E'* in glass region compared with neat epoxy resin, consistent with the results of CNF reinforced epoxy resin in an earlier report [39]. Continuous improvement of *E'* is obtained as the filler loading increases in the testing range. Notably, *E'* (at 50 °C) of the composites with 0.4 wt% load of p-CNFs and m-CNFs reach the values of 2535 and 2630 MPa, which are about 14 and 19% higher than that of neat epoxy resin, respectively. Loss modulus represents the energy dissipation due to the internal friction related to the motion of the polymer chain. Figs.7b and e show that there are almost no other relaxations except one peak corresponding to glass transition in each curve. This phenomenon indicates that every resin system is fairly a homogeneous phase. In addition, the loss modulus of both series of composites also increases with CNFs content, which may be due to that, as the temperature increases, the incorporation of CNFs provides

additional internal friction between CNFs and polymer chain besides the friction between the epoxy molecules [40,41].

The tan δ is defined as the ratio of loss modulus to the storage modulus, and the peak of the tan δ versus temperature curve is often used to determine the glass transition temperature (T_g). As expected, the neat epoxy resin shows high T_g value (228 °C) due to the tetra-functional epoxy monomer. All the composites show T_g values (225-234 °C) comparable to that of neat epoxy resin, indicating that the incorporation of both CNF fillers has no significant influence on the overall crosslinking density of the epoxy matrix. It has been reported that a decrease in crosslinking density of epoxy thermosets commonly improves their toughness due to the formation of a looser, more mobile network [7,15,42]. Our T_g results obtained from DMA and DSC (Table S3 in Supplementary materials) verify that the toughness enhancements of the two series of composites are not caused by the changes in crosslinking degree of the epoxy matrix.

Thermal stability of neat epoxy and the composites was evaluated by TGA in an air atmosphere. The TGA curves are shown in Fig. 8 and the data are summarized in Table 1. All the samples are observed to degrade in two stages and display similar T_d values in the range of 296–311 °C. These two degradation stages are related to the degradation of aliphatic (first stage) and aromatic (second stage) components of epoxy matrix, respectively [13]. It is noticed that the degradation rate of the composites is obviously slower than that of neat epoxy resin in the second stage within 400-600 °C, indicating that the incorporation of CNFs into epoxy offers a stabilizing effect against the decomposition [13,20].

4. Conclusions

Triazole-functionalized CNFs (m-CNFs) have been prepared by one-step arylation with diazonium salts generated in situ. The results from FTIR, XPS, TGA and elemental analysis

indicate that the triazole groups have been successfully grafted on the CNF surface. As evidenced by various microscopic observation and DSC, the functionalization of the CNFs not only provides chemical affinity for their effective dispersion in the epoxy matrix, but also contributes to the formation of a robust interface between the CNFs and epoxy matrix through chemical bonding. Consequently, m-CNFs show superior ability in toughening the epoxy resin over p-CNFs. The addition of only 0.4 wt% m-CNFs yields 41 and 80% enhancement in critical stress intensity factor (K_{IC}) and the critical strain energy release rate (G_{IC}), respectively. Several typical toughening mechanisms, including the unraveling of the graphene layers of the stacked-cup CNFs, have been observed from the fractured surfaces of m-CNF/epoxy composites by SEM. At last, DSC, DMA and TGA tests indicate that the incorporation of p-CNFs and m-CNFs has insignificant influence on the thermal properties of the composites.

Acknowledgment

This work was supported by Science and Engineering Research Council of the Agency for Science, Technology and Research (A*STAR) Singapore under Grant No. 11 2300 4027.

Appendix A. Supplementary materials

Supplementary data associated with this article can be found in the online version.

References

[1] Thio YS, Wu JX, Bates FS. Epoxy toughening using low molecular weight poly(hexylene oxide)-poly(ethylene oxide) diblock copolymers. Macromolecules 2006;39(21):7187-7189.
[2] Bagheri R, Marouf BT, Pearson RA. Rubber-toughened epoxies: a critical review. Polym Rev 2009;49(3):201-225.
[3] Tripathy R, Ojha U, Faust R. Polyisobutylene modified bisphenol A diglycidyl ether based epoxy resins possessing improved mechanical properties. Macromolecules 2011;44(17):6800-6809.
[4] Liu J, Thompson ZJ, Sue HJ, Bates FS, Hillmyer MA, Dettloff M, et al. Toughening of epoxies with block copolymer micelles of wormlike morphology. Macromolecules 2010;43(17):7238-7243.
[5] Johnsen BB, Kinloch AJ, Mohammed RD, Taylor AC, Sprenger S. Toughening mechanisms of nanoparticle-modified epoxy polymers. Polymer 2007;48(2):530-541.

[6] Rafiee MA, Rafiee J, Wang Z, Song HH, Yu ZZ, Koratkar N. Enhanced mechanical properties of composites at low graphene content. ACS Nano 2009;3(12):3884−3890.
[7] Martinez-Rubi Y, Ashrafi B, Guan JW, Kingston C, Johnston A, Simard B, et al. Toughening of epoxy matrices with reduced single-walled carbon nanotubes. ACS Appl Mater Interfaces 2011;3(7):2309-2317.
[8] Shadlou S, Alishahi E, Ayatollahi MR. Fracture behavior of epoxy nanocomposites reinforced with different carbon nano-reinforcements. Compos Struct 2013;95:577-581.
[9] Yang SY, Lin WN, Huang YL, Tien HW, Wang JY, Ma CC, et al. Synergetic effects of graphene platelets and carbon nanotubes on the mechanical and thermal properties of epoxy. Carbon 2011;49(3):793-803.
[10] Fang M, Zhang Z, Li JF, Zhang HD, Lu HB, Yang YL. Constructing hierarchically structured interphases for strong and tough epoxy nanocomposites by amine-rich graphene surfaces. J Mater Chem 2010;20(43):9635-9643.
[11] Xu SA, Wang GT, Mai YW. Effect of hybridization of liquid rubber and nanosilica particles on the morphology, mechanical properties, and fracture toughness of epoxy composites. J Mater Sci 2013;48(9):3546-3556.
[12] Chatterjee S, Nafezarefi F, Tai NH, Schlagenhauf L, Nuesch FA, Chu BTT. Size and synergy effects of nanofiller hybrids including graphene nanoplatelets and carbon nanotubes in mechanical properties of epoxy composites. Carbon 2012;50(15):5380-5386.
[13] Wang DH, Sihn S, Roy AK, Baek JB, Tan LS. Nanocomposites based on vapor-grown carbon nanofibers and an epoxy: functionalization, preparation and characterization. Eur Polym J 2010;46(7):1404-1416.
[14] Lawrence JG, Berhan LM, Nadarajah A. Elastic properties and morphology of individual carbon nanofibers. ACS Nano 2008;2(6):1230-1236.
[15] Palmeri ML, Putz KW, Brinson LC. Sacrificial bonds in stacked-cup carbon nanofibers: biomimetic toughening mechanisms for composite systems. ACS Nano 2010;4(7):4256-4264.
[16] Al-Saleh MH, Sundararaj U. Review of the mechanical properties of carbon nanofiber/ polymer composites. Composites Part A 2011;42(12):2126-2142.
[17] Choi YK, Sugimoto K, Song SM, Gotoh Y, Ohkoshi Y, Endo M. Mechanical and physical properties of epoxy composites reinforced by vapor grown carbon nanofibers. Carbon 2005;43 (10):2199-2208.
[18] Rodriguez AJ, Guzman ME, Lim CS, Minaie B. Mechanical properties of carbon nanofiber/ fiber-reinforced hierarchical polymer composites manufactured with multiscale-reinforcement fabrics. Carbon 2011;49(3):937-948.
[19] Ahn SN, Lee HJ, Kim BJ, Tan LS, Beak JB. Epoxy/amine-functionalized short-length vapor-grown carbon nanofiber composites. J Polym Sci Part A: Polym Chem 2008;46:7473–82.
[20] Zhu JH, Wei SY, Ryu J, Budhathoki M, Liang G, Guo ZH. In situ stabilized carbon nanofiber (CNF) reinforced epoxy nanocomposites. J Mater Chem 2010;20(23):4937-4948.
[21] Nie YR, Hubert T. Effect of carbon nanofiber (CNF) silanization on the properties of CNF/epoxy nanocomposites. Polym Int 2011;60(11):1574-1580.
[22] Zhu Y, Bakis CE, Adair JH. Effects of carbon nanofiller functionalization and distribution on interlaminar fracture toughness of multi-scale reinforced polymer composites. Carbon 2012; 50(3):1316-1331.
[23] Ryu BY, Emrick T. Bisphenol-1,2,3-triazole (BPT) epoxies and cyanate esters: synthesis and self-catalyzed curing. Macromolecules 2011;44(14):5693-5700.

[24] Bahr JL, Tour JM. Highly functionalized carbon nanotubes using in situ generated diazonium compounds. Chem Mater 2001;13(11):3823-3824.
[25] Menard-Moyon C, Fabbro C, Prato M, Bianco A. One-pot triple functionalization of carbon nanotubes. Chem-Eur J 2011;17(11):3222–7.
[26] Meador MAB, Vivod SL, McCorkle L, Quade D, Sullivan RM, Ghosn LJ, et al. Reinforcing polymer cross-linked aerogels with carbon nanofibers. J Mater Chem 2008;18(16):1843-1852.
[27] Wei J, Hing P. Optical behavior of reactive sputtered carbon nitride films. J Appl Phys 2002;91(5):2812-2817.
[28] Bhunia P, Hwang E, Min M, Lee J, Seo S, Some S, et al. A non-volatile memory device consisting of graphene oxide covalently functionalized with ionic liquid. Chem Commun 2012; 48(6):913-915.
[29] Bhargava G, Ramanarayanan TA, Bernasek SL. Imidazole-Fe interaction in an aqueous chloride medium: effect of cathodic reduction of the native oxide. Langmuir 2010;26(1):215-219.
[30] Yurdakul S, Tanribuyurdu S. FT-IR, FT-Raman, vibrational assignments, and density functional studies of 1,2,4-triazole-3-carboxylic acid, and its tautomers, dimmers. Struct Chem 2012;23(2):433-440.
[31] Pagacz-Kostrzewa M, Bronisz R, Wierzejewska M. Theoretical and matrix isolation FTIR studies of 3-amino-1,2,4-triazole and its isomers. Chem Phys Lett 2009;473(4-6):238-246.
[32] Montserrat S, Flaque C, Calafell M, Andreu G, Malek J. Influence of the accelerator concentration on the curing reaction of an epoxy-anhydride system. Thermochi Acta 1995;269: 213-229.
[33] Rocks J, Rintoul L, Vohwinkel F, George G. The kinetics and mechanism of cure of an amino-glycidyl epoxy resin by a co-anhydride as studied by FT-Raman spectroscopy. Polymer 2004;45(20): 6799-6811.
[34] Gonzalez-Dominguez JM, Gonzalez M, Anson-Casaos A, Diez-Pascual AM, Gomez MA, Martinez MT. Effect of various aminated single-walled carbon nanotubes on the epoxy cross-linking reactions. J Phys Chem C 2011;115(15):7238–7248.
[35] Wang S, Liang Z, Liu T, Wang B, Zhang C. Effective aminofunctionalization of carbon nanotubes for reinforcing epoxy polymer composites. Nanotechnology 2006;17(6):1551–1557.
[36] Fiedler B, Gojny FH, Wichmann MHG, Nolte MCM, Schulte K. Fundamental aspects of nano-reinforced composites. Compos Sci Technol 2006;66(16):3115-3125.
[37] Hwang GL, Shieh YT, Hwang KC. Efficient load transfer to polymer-grafted multiwalled carbon nanotubes in polymer composites. Adv Funct Mater 2004;14(5):487-491.
[38] Gojny FH, Wichmann MHG, Fiedler B, Schulte K. Influence of different carbon nanotubes on the mechanical properties of epoxy matrix composites – A comparative study. Comps Sci technol 2005;65(15-16):2300-2313.
[39] Sun LH, Ounaies Z, Gao XL, Whalen CA, Yang ZG. Preparation, characterization, and modeling of carbon nanofiber/epoxy nanocomposites. J Nanomater 2011;2011:307589 1-8.
[40] Hsueh HB, Chen CY. Preparation and properties of LDHs/epoxy nanocomposites. Polymer 2003;44(18):5275-5283.
[41] Rahman MM, Hosur M, Ludwick AG, Zainuddin S, Kumar A, Trovilion J, et al. Thermo-mechanical behavior of epoxy composites modified with reactive polyol diluent and randomly-oriented amino-functionalized multi-walled carbon nanotubes. Polym Test 2012;31(6):777-784.
[42] Crawford E, Lesser AJ. The effect of network architecture on the thermal and mechanical behavior of epoxy resins. J Polym Sci Part B: Polym Phys 1998;36(8):1371-1382.

Captions for Figures

Fig. 1 Synthesis route of m-CNFs and formulas of epoxy and hardener used in this study.

Fig. 2 (a) C1 XPS spectra of p-CNFs; (b) C1 XPS spectra of m-CNFs; (c) N1 XPS spectra of m-CNFs; (d) FTIR spectra and (e) TGA curves in a nitrogen atmosphere of p-CNFs and m-CNFs.

Fig. 3 Tensile strength (a), Young's modulus (b) and fracture toughness (c and d) of neat epoxy resin and the composites.

Fig. 4 Optical micrographs (magnification = 500) of p-CNFs (a) and m-CNFs (b) in the epoxy/ anhydride mixture before curing and those of p-CNFs (c) and m-CNFs (d) in the epoxy matrix after curing; TEM micrographs of p-CNF/epoxy (e) and m-CNF/epoxy (f) composites. The filler loading of all the samples is 0.4 wt %.

Fig. 5 SEM micrographs of fractured surfaces of neat epoxy resin (a, b), p-CNF/epoxy (c, d) and m-CNF/epoxy (e, f) composites at low and high magnification.

Fig. 6 SEM micrographs of the fractured surfaces of m-CNF/epoxy composites showing CNF across a crack (a); CNF rupture (b), CNF pull out and localized debonding (c), possible unraveling of CNF (d and inset). The m-CNF content is 0.4 wt%.

Fig. 7 Storage modulus, loss mudlus and tan δ versus temperature curves of p-CNF/epoxy (a, b and c) and m-CNF/epoxy (d, e and f) composites in comparison with that of neat epoxy resin.

Fig. 8 TGA curves of neat epoxy resin and composites in an air atmosphere

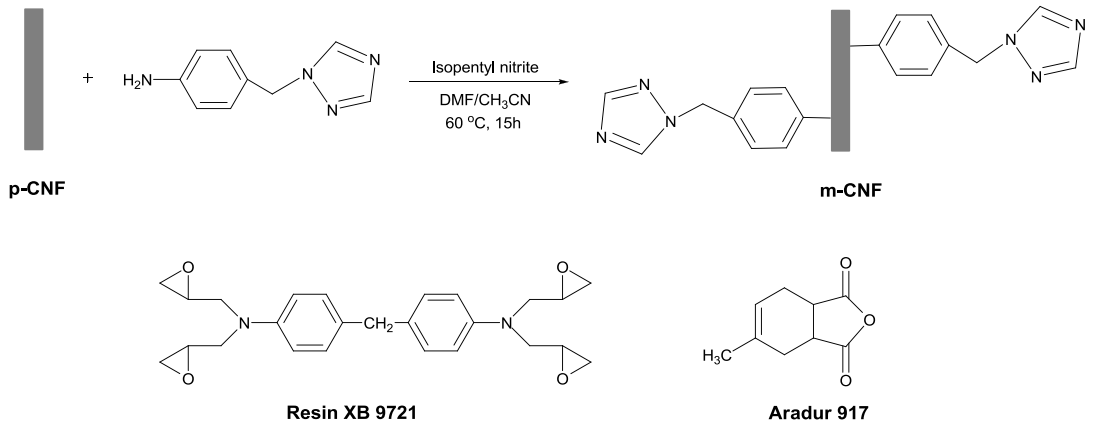

Fig. 1. Synthesis route of m-CNFs and formulas of epoxy and hardener used in this study

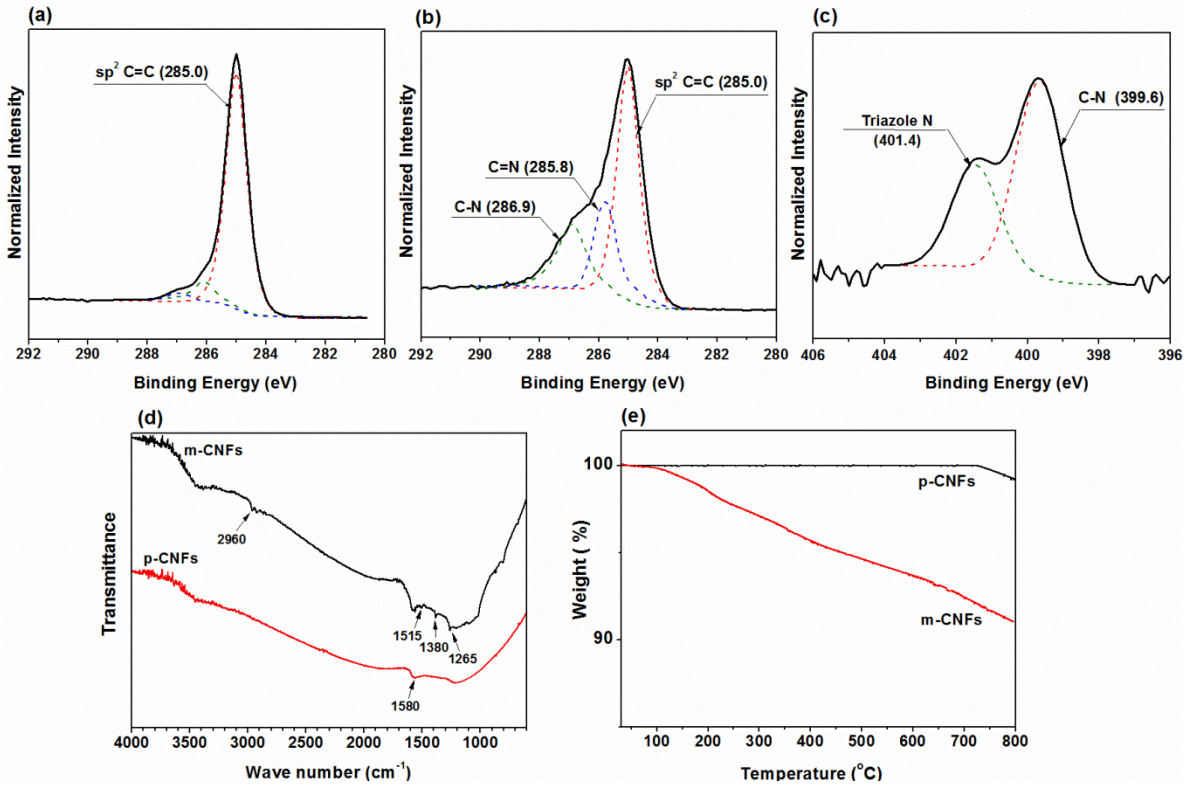

Fig. 2. (a) C1 XPS spectra of p-CNFs; (b) C1 XPS spectra of m-CNFs; (c) N1 XPS spectra of m-CNFs; (d) FTIR spectra and (e) TGA curves in a nitrogen atmosphere of p-CNFs and m-CNFs.

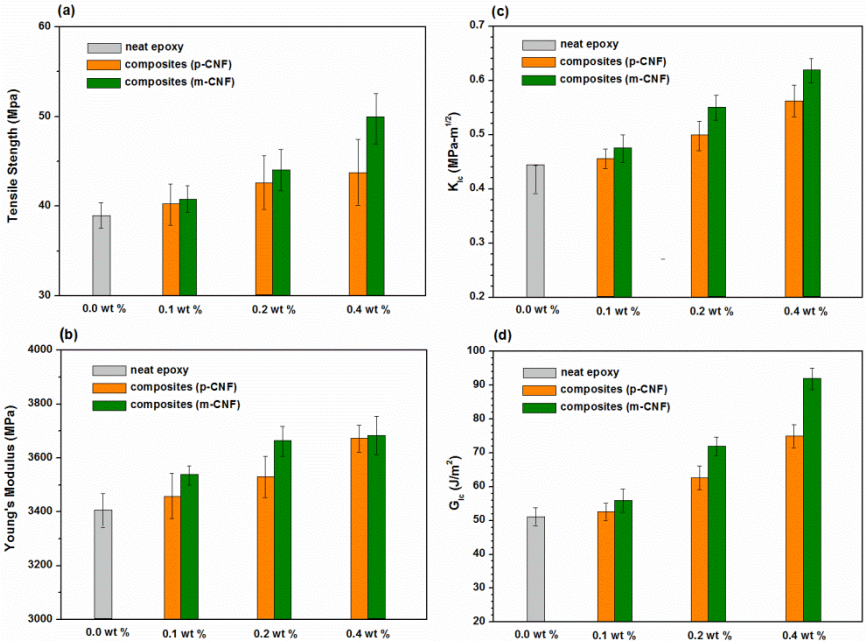

Fig. 3. Tensile strength (a), Young's modulus (b) and fracture toughness (c and d) of neat epoxy resin and the composites.

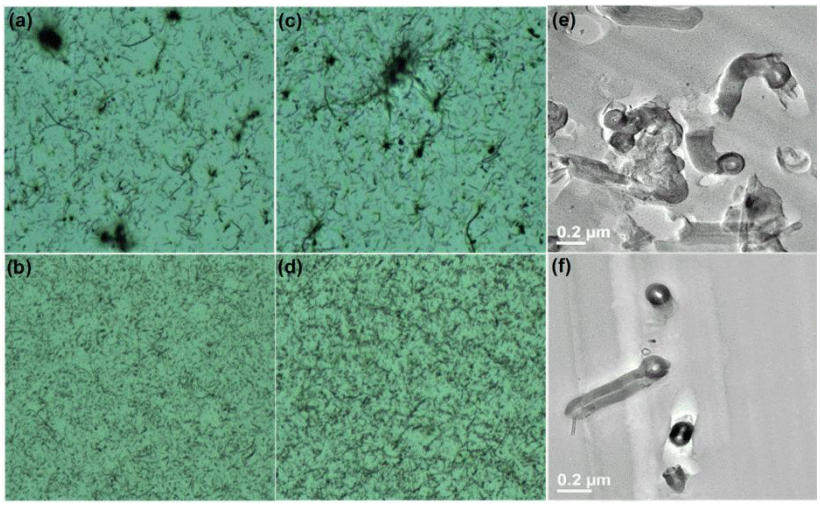

Fig. 4. Optical micrographs (magnification = 500) of p-CNFs (a) and m-CNFs (b) in the epoxy/ anhydride mixture before curing and those of p-CNFs (c) and m-CNFs (d) in the epoxy matrix after curing; TEM micrographs of p-CNF/epoxy (e) and m-CNF/epoxy (f) composites. The filler loading of all the samples is 0.4 wt %.

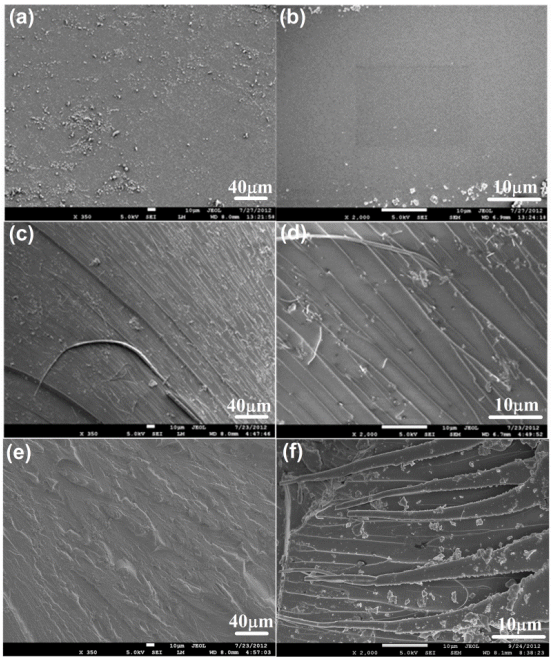

Fig. 5. SEM micrographs of fractured surfaces of neat epoxy resin (a, b), p-CNF/epoxy (c, d) and m-CNF/epoxy (e, f) composites at low and high magnification.

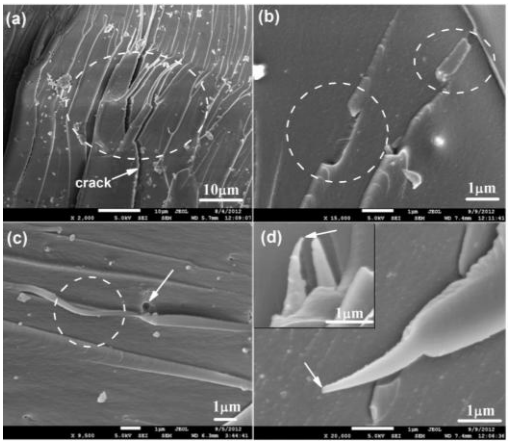

Fig. 6. SEM micrographs of the fractured surfaces of m-CNF/epoxy composites showing CNF across a crack (a); CNF rupture (b), CNF pull out and localized debonding (c), possible unraveling of CNF (d and inset). The m-CNF content is 0.4 wt%.

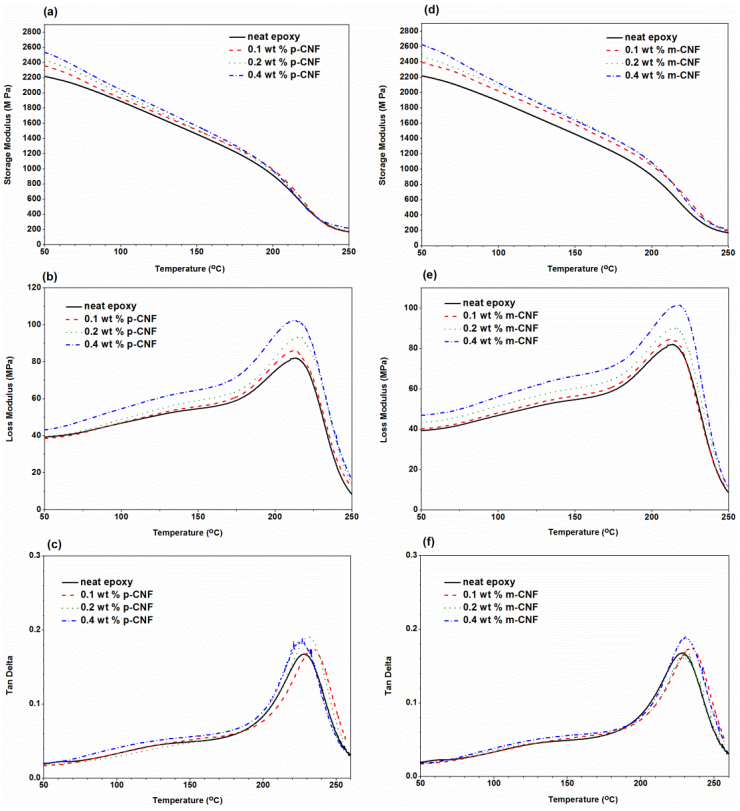

Fig. 7. Storage modulus, loss modulus and tan δ versus temperature curves of p-CNF/epoxy (a, b and c) and m-CNF/epoxy (d, e and f) composites in comparison with that of neat epoxy resin.

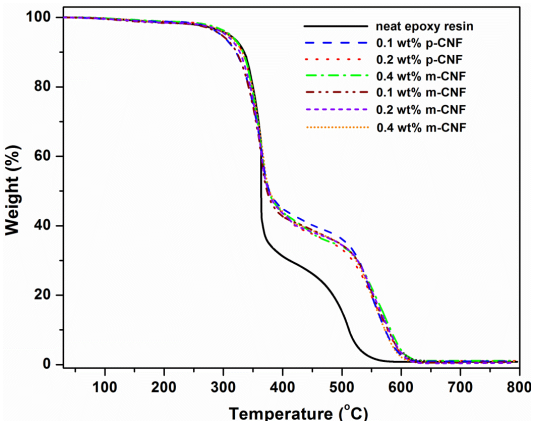

Fig. 8. TGA curves of neat epoxy resin and composites in an air atmosphere.

Table 1 DMA and TGA results of neat epoxy resin and the composites

Filler Loading	Storage Modulus		T_g (°C)	T_d[a] (°C)
	50°C (MPa)	200°C (MPa)		
Neat epoxy	2215	914	228	307
0.1 wt % p-CNFs	2340	989	233	296
0.1 wt % m-CNFs	2400	1047	234	296
0.2 wt % p-CNFs	2417	965	231	310
0.2 wt % m-CNFs	2482	1075	229	304
0.4 wt % p-CNFs	2535	974	225	311
0.4 wt % m-CNFs	2630	1087	230	308

[a] Temperature at 5 % weight loss

Toughening of epoxies by covalently anchoring triazole-functionalized stacked-cup carbon nanofibers

Wanshuang Liu, Junhua Kong, Weilong Eric Toh, Rui Zhou, Guoqiang Ding, Shu Huang, Yuliang Dong, Xuehong Lu*

School of Materials Science and Engineering, Nanyang Technological University, 50 Nanyang Avenue, Singapore 639798, Singapore

*Corresponding author: Tel: +65 9847 6690

E-mail address: asxhlu@ntu.edu.sg (X. Lu)

(Supplementary materials)

1. Elemental analysis

Table S1 Elemental analysis for m-CNFs

Element Name	Nitrogen	Hydrogen	Carbon	Sulphur	Difference
Atomic Content (wt %)	3.02	0.80	88.99	0.25	6.92

In the elemental analysis, the amounts of metals and oxygen were not examined, which is why the total percentage does not add up to 100%.

2. DSC

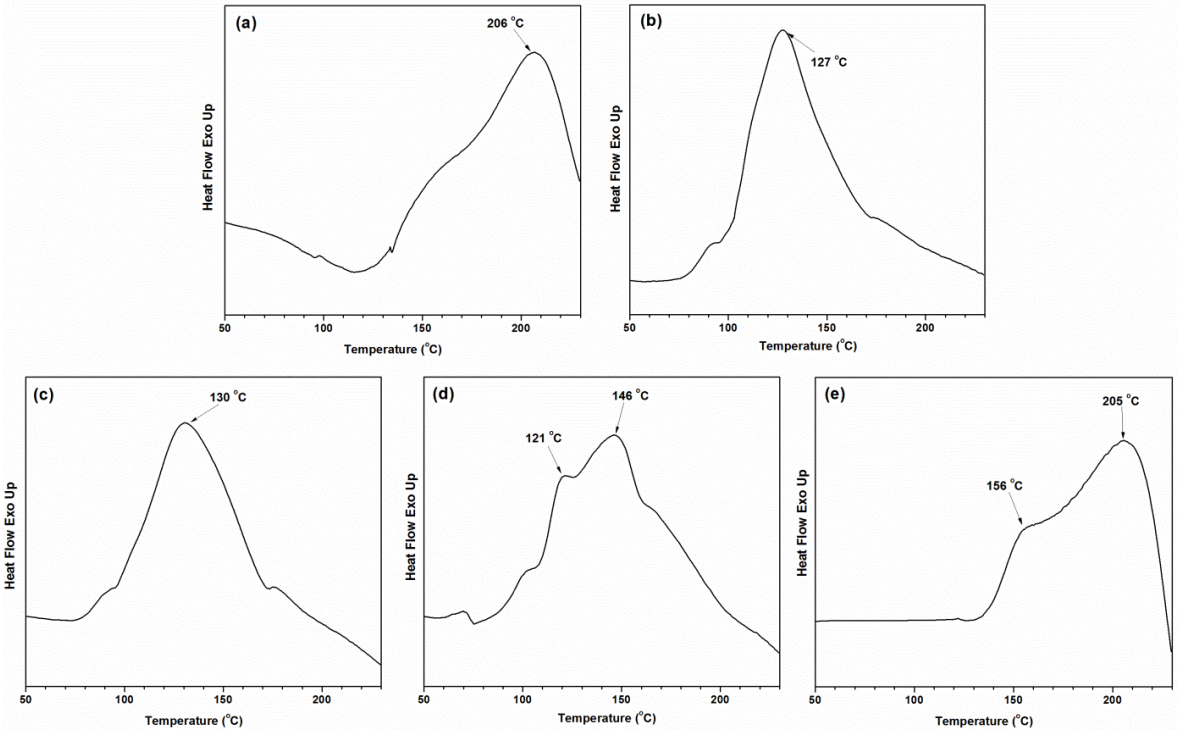

Fig. S1 - DSC of the curing reactions: (a) neat epoxy without catalyst; (b) neat epoxy with catalyst; (c) p-CNF/epoxy with catalyst; (d) m-CNF/epoxy with catalyst; (e) m-CNF/epoxy without catalyst. The CNFs content is 0.4 wt%.

Table S2 DSC data of the curing reaction

Epoxy system	Exotherm (J/g)
Pure epoxy without catalyst	41
m-CNF/epoxy without catalyst	106
m-CNF/epoxy with catalyst	170
p-CNF/epoxy with catalyst	272
Pure epoxy with catalyst	312

The data in Table S2 correspond to areas of exothermic peaks in the Fig. S1, and the temperature ramps from 50 to 220°C at a rate of 3°C/min.

Table S3 DSC data of the cured neat epoxy and composites

Epoxy system	Exotherm (J/g)
Pure epoxy	11.4
p-CNF/epoxy	3.9
m-CNF/epoxy	6.7

The data in Table S3 correspond to areas of exothermic peaks in DSC of cured neat epoxy and composites, and temperature ramps from 150 to 280°C at a rate of 3°C/min.

3. Mechanical properties

Table S4 Data of mechanical properties of neat epoxy and composites

Sample	Tensile strength (MPa)	Young's modulus (Mpa)	K_{IC} (MPa $m^{1/2}$)	G_{IC} (J/m^2)
Neat epoxy	39.0 ± 1.5	3407 ± 62	0.444 ± 0.024	51.1 ± 2.8
0.1 wt% p-CNF	40.3 ± 2.0	3456 ± 88	0.455 ± 0.018	52.6 ± 2.5
0.2 wt% p-CNF	42.6 ± 3.1	3530 ± 77	0.500 ± 0.026	62.6 ± 3.6
0.4 wt% p-CNF	43.7 ± 3.8	3670 ± 52	0.562 ± 0.029	74.8 ± 3.5
0.1 wt% m-CNF	40.8 ± 1.5	3540 ± 30	0.475 ± 0.025	55.8 ± 3.2
0.2 wt% m-CNF	44.1 ± 2.2	3665 ± 54	0.551 ± 0.020	72.1 ± 2.4
0.4 wt% m-CNF	50.0 ± 2.5	3685 ± 70	0.619 ± 0.022	91.9 ± 3.0

4. SEM

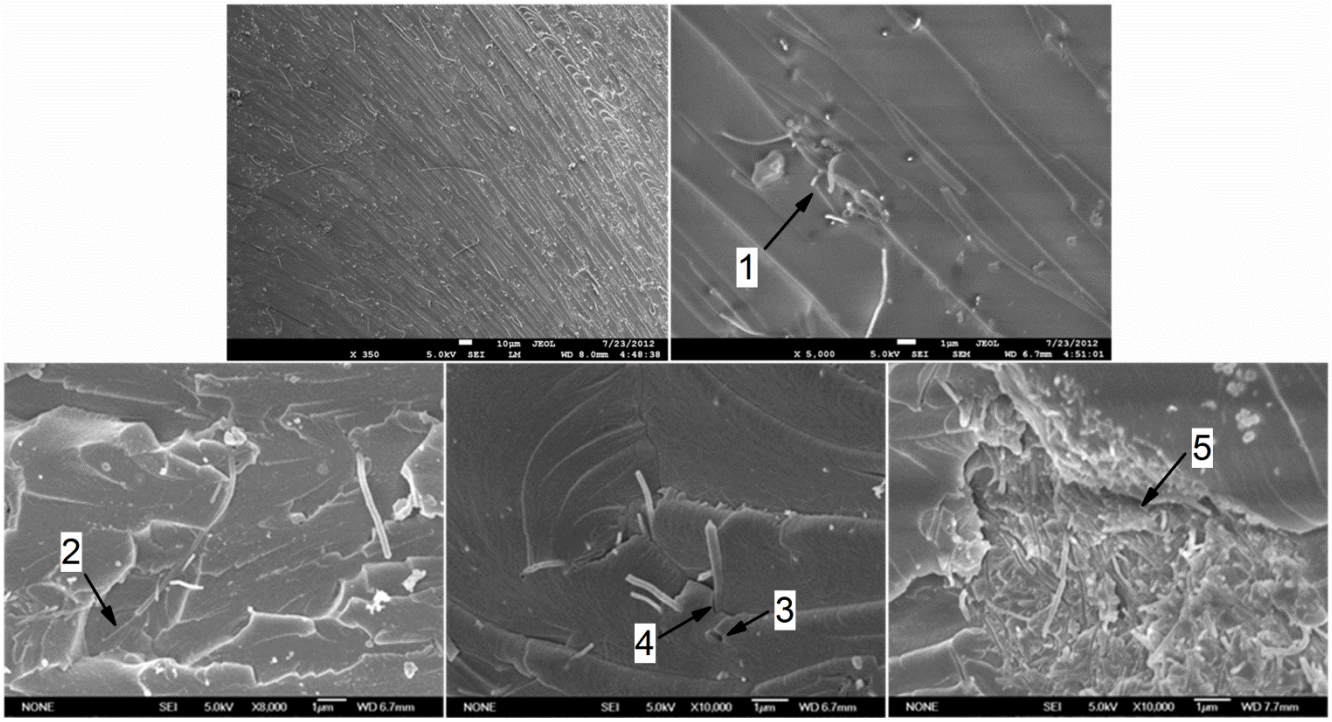

Fig. S2 - SEM micrographs obtained from fracture surface of p-CNF/epoxy composites with 0.4 wt% filler loading. (1) small aggregation of CNF; (2) CNF rupture and debonding; (3) CNF pull out; (4) a small gap between a CNF and matrix; (5) a crack derived from aggregation of CNF.